Observer Quality as a Resource Constraint in Quantum Darwinism: Optimal Decoding, ε-Approximate Spectrum Broadcast Structure, and a Central-Spin Worked Example

Alia Wu
Risk Efficacy & Redline Rising
wut08@nyu.edu
ORCID: 0009-0005-4424-102X

February 7, 2026

Abstract

Quantum Darwinism (QD) and Spectrum Broadcast Structure (SBS) formalize a mechanism by which many observers can learn the same classical pointer value of a system by measuring different fragments of its environment. Most QD analyses treat the observer as idealized: unlimited access, perfect calibration, and no temporal constraints. This paper introduces an explicit *observer quality* parameterization and propagates it through redundancy and objectivity statements in a way that remains stable under an explicit ε-SBS trace-distance error model.

Our main technical contributions are: (i) a decoder-level, tight (Chernoff-optimal) sample-complexity characterization for the number of environmental fragments needed to infer a pointer value under a calibrated observer model, (ii) a data-processing theorem showing that calibration noise (modeled as a CPTP channel) degrades the quantum Chernoff exponent, and (iii) an ε-robustness theorem upgrading ideal-SBS sample-complexity bounds to approximate-SBS states with additive error control.

We ground the formalism in a fully worked open-system example: a central-spin pure-dephasing model whose conditional fragment states can be computed analytically, yielding explicit formulas for the observer parameters (R_O, C_O, τ_O) as functions of couplings, readout noise, and acquisition time. We also highlight a sharp performance gap between collective (coherent) decoding and product-measurement decoding for pure-state records, directly linking *quantum memory horizon* to redundancy. Finally, to connect this physics formalism to the DLN observer-quality framework, we introduce a three-state stage index $q_O \in \{q_{\mathrm{D}}, q_{\mathrm{L}}, q_{\mathrm{N}}\}$ mapping Dot/Linear/Network stages to memoryless, product, and collective decoding classes.

We then prove three dynamical results about *observer topology* over time: (A) a dynamical redundancy theorem showing that the long-run effective Chernoff exponent depends on the observer's revision topology $\mathcal{R}_O$, with full-cycle revision achieving the adaptive optimum while expand-only revision collapses permanently to the linear baseline; (B) an "inverted sophistication" theorem showing that an *unmonitored* collective decoder can be strictly worse than optimal product decoding below a critical coherence fraction; and (C) a pointer-accessibility proposition formalizing how the DLN stage determines which pointer distinctions are resolvable from a fixed fragment budget, providing an operational basis for observer-designed control of accessible quantum outcomes.

1 Introduction

Quantum Darwinism proposes that classical objectivity arises when information about a preferred pointer observable of a system is redundantly encoded in the environment [1–3]. A complementary structural characterization is Spectrum Broadcast Structure [4, 5], and strong-QD variants connect entropic and geometric criteria [5, 6].

A persistent modeling gap is that *observers are usually treated as ideal*. Yet in realistic experiments or cognitive settings, an observer may: (i) access only a fraction of environment fragments, (ii) have imperfect measurement calibration, and (iii) be limited by a temporal integration horizon (finite memory or pointer stability). There is substantial prior work on non-idealities in the *environment* (e.g., "hazy" environments [7]) and on generic emergence of objectivity [8, 9], but the observer itself is rarely parameterized at the same level of explicitness.

Scope of this paper. We restrict to a single core task: *observer-relative redundancy/objectivity statements* in QD/SBS when the observer is explicitly modeled by a quality triple

$$Q_O = (R_O, \Lambda_O, \tau_O),$$

where R_O is an access fraction, Λ_O is a calibration channel applied to each accessed fragment prior to readout, and τ_O is an acquisition or memory horizon. For interpretability (and to align with existing QD language) we also extract a scalar *calibration index* C_O from Λ_O in the binary case.

Why an ε-SBS error model. Many QD/SBS derivations assume conditional i.i.d. record models. Instead, we start from an explicit trace-distance approximation: the actual joint state $\rho_{S\mathcal{E}}$ is within ε in trace distance of an *ideal* SBS state $\sigma_{S\mathcal{E}}$. We then push sample-complexity statements through this approximation using data processing and decision-theoretic continuity bounds.

Observer topology over time. The quality triple Q_O captures *static* limitations within a single observational episode. However, in realistic QD/SBS protocols the observation model may be non-stationary (e.g., coherence loss across the fragment register, drifting calibration, or regime switching in the environment), so the observer's capacity to *revise* its decoding assumptions becomes a second, structurally distinct resource. Motivated by the Dot–Linear–Network (DLN) revision-graph formalism [10], we introduce an observer-specific revision topology $\mathcal{R}_O$ over decoder models and establish how this topology governs the long-run redundancy rate. This yields three results (Sec. 9): dynamical redundancy as a topological invariant of $\mathcal{R}_O$ (Result A), inverted sophistication for unmonitored collective decoding (Result B), and pointer accessibility as a stage-dependent resolution bound (Result C).

2 Related work and positioning

This paper builds on three strands:

1. **QD and SBS foundations.** The environment-as-witness framing originates in Ollivier et al. [1] and is synthesized by Zurek [2], Blume-Kohout and Zurek [3]. SBS provides a structural notion of objectivity [4], and a unifying review is Korbicz [5]. Strong-QD links entropic and structural conditions [6].

2. **Non-ideal environments and fragment size.** "Hazy" environments reduce redundancy and record capacity [7]. Photon-scattering models exhibit huge redundancy in everyday environments [11, 12].

3. **Hypothesis testing and optimal decoding.** Binary quantum hypothesis testing is classical material [13, 14]. The quantum Chernoff bound characterizes the optimal asymptotic error exponent [15, 16]. These tools are natural for QD because "learning the pointer value" is precisely a discrimination task between conditional fragment states.

We also connect to recent resource-theoretic and operational approaches emphasizing *accessible information* rather than mutual information [17]. Experimental signatures of quantum Darwinism have been observed in photonic [18] and spin-based platforms; the observer-quality framework developed here provides a route to predicting how detector limitations affect such experiments quantitatively.

3 Setup: SBS, ε-SBS, and observer quality

3.1 Spectrum Broadcast Structure and its approximation

Let S be the system and $\mathcal{E} = \mathcal{E}_1 \otimes \cdots \otimes \mathcal{E}_N$ a decomposition of the environment into fragments. We focus on a classical pointer random variable X taking values in a finite alphabet $\mathcal{X}$ (often $\mathcal{X} = \{0, 1\}$).

Definition 1 (SBS state)**.** A joint state $\sigma_{S\mathcal{E}}$ has *spectrum broadcast structure* (SBS) with respect to pointer basis $\{|x\rangle\}_{x\in\mathcal{X}}$ if it can be written as

$$\sigma_{S\mathcal{E}} = \sum_{x\in\mathcal{X}} p_x \, |x\rangle\langle x|_S \otimes \bigotimes_{k=1}^{N} \sigma_{\mathcal{E}_k}^{(x)}, \tag{1}$$

where p is a probability distribution and, for each fragment k, the conditional states $\{\sigma_{\mathcal{E}_k}^{(x)}\}_{x\in\mathcal{X}}$ have mutually orthogonal supports (perfect distinguishability) [4, 5].

Definition 2 (ε-SBS)**.** A state $\rho_{S\mathcal{E}}$ is *ε-SBS* if there exists an SBS state $\sigma_{S\mathcal{E}}$ such that

$$D_{\mathrm{tr}}(\rho_{S\mathcal{E}}, \sigma_{S\mathcal{E}}) \le \varepsilon, \qquad D_{\mathrm{tr}}(\rho, \sigma) := \tfrac{1}{2} \left\|\rho - \sigma\right\|_1 .$$

3.2 Observer quality

An observer interacts only with a subset of fragments and through an imperfect instrument.

Definition 3 (Observer quality)**.** An observer is specified by a quality triple

$$Q_O = (R_O, \Lambda_O, \tau_O),$$

where:

1. $R_O \in [0, 1]$ is an *access fraction*: out of N fragments, O can access at most $m_{\max} = \lfloor R_O N \rfloor$ fragments in a given observational episode;

2. Λ_O is a CPTP map acting on each accessed fragment, representing calibration noise, coarse-graining, or any pre-measurement processing;

3. τ_O is a temporal horizon (memory, stability, or acquisition time). In the central-spin model (Sec. 7), it is mapped to an acquisition time budget and a pointer-stability constraint.

When $\mathcal{X} = \{0, 1\}$, we can compress Λ_O to a scalar "single-fragment calibration" index.

Definition 4 (Binary calibration index)**.** Let ρ_0, ρ_1 be the two conditional states of a single accessed fragment after Λ_O, and assume equal priors. Define

$$C_O := 1 - P_e^\star(\rho_0, \rho_1), \qquad P_e^\star(\rho_0, \rho_1) = \tfrac{1}{2}\left(1 - \tfrac{1}{2}\left\|\rho_0 - \rho_1\right\|_1\right), \tag{2}$$

where $P_e^\star$ is the Helstrom-optimal single-copy Bayes error [13, 14]. Then $C_O \in [\frac{1}{2}, 1]$.

3.3 DLN stage index and three discrete observer-quality states

The resource triple $Q_O = (R_O, \Lambda_O, \tau_O)$ is a *continuous* parameterization of observer limitations: it specifies how many fragments can be accessed, how each accessed record is distorted by calibration, and how long the observer can integrate across fragments. For several questions in quantum Darwinism it is also useful to coarse-grain observers into a small number of *information-processing regimes*. Motivated by the Dot–Linear–Network (DLN) observer-quality framework, which formalizes stage differences via belief-dependency graphs and a revision graph over model space [10], we introduce a three-valued stage variable

$$q_O \in \{q_{\mathrm{D}}, q_{\mathrm{L}}, q_{\mathrm{N}}\} \equiv \{0, 1, 2\}.$$

In this paper, q_O is defined operationally by the class of admissible decoding procedures on an m-fragment register within the observer's temporal horizon.

Definition 5 (Three q-states as decoder classes)**.** Fix a fragment set $A \subseteq \{1, \ldots, N\}$ with $|A| = m$ and conditional states $\rho_A^{(x)} := \bigotimes_{k\in A} \Lambda_O(\sigma_{\mathcal{E}_k}^{(x)})$ (SBS witness experiment, $\mathcal{X} = \{0, 1\}$). A *decoder* is a measurement–decision procedure producing an estimate $\widehat{X} \in \{0, 1\}$ from the m-fragment quantum register. We define three nested decoder classes:

(i) q_{D} **(Dot).** *Single-fragment / memoryless decoding.* The decoder acts on at most one fragment at a time and retains no state across fragments. Equivalently, the effective hypothesis test is restricted to a single-copy test on $\Lambda_O(\sigma_{\mathcal{E}_k}^{(x)})$ for some k.

(ii) q_{L} **(Linear).** *Product decoding with classical postprocessing.* The decoder applies a product POVM across fragments, $M = \bigotimes_{k\in A} M_k$, followed by an arbitrary classical decision rule on the measurement outcomes. This class captures "branch-by-branch" processing: each fragment contributes evidence independently, and no quantum-coherent joint processing across distinct fragments is available.

(iii) q_{N} **(Network).** *Collective decoding.* The decoder may apply an arbitrary POVM on the joint register $\bigotimes_{k\in A} \mathcal{E}_k$ (equivalently, any collective m-copy hypothesis test), attaining Chernoff-optimal error exponents when the record model is i.i.d.

Remark 1 (Relation to finite-resource sample complexity)**.** The results below quantify how the required fragment count m scales with the error target δ and with calibration noise. This is a finite-resource regime in the sense of non-asymptotic quantum information theory [19, 20]. Recent work has sharpened the *sample-complexity* viewpoint in quantum hypothesis testing and related tasks [21]. In our setting, the relevant operational distinction is whether $q_O = q_{\mathrm{L}}$ or $q_O = q_{\mathrm{N}}$: under q_{N} collective decoding achieves the quantum Chernoff exponent, while under q_{L} the achievable exponent can be strictly smaller (Cor. 1).

Table 1: Mapping between three observer-quality q-states and DLN stages. The DLN column follows the graph-theoretic stage definitions in Wu [10]. The decoding column specifies the admissible measurement class on m accessed fragments in this paper.

q_O	DLN stage	DLN representational signature	Operational signature (QD decoding)
q_{D}	Dot	No persistent belief-dependency graph ($G = \emptyset$); reactive policy.	Single-fragment or memoryless decoding; no $m > 1$ aggregation.
q_{L}	Linear	Null belief graph over evidence nodes; no cross-node information propagation.	Product measurements with classical postprocessing; no coherent joint decoding across fragments.
q_{N}	Network	Shared latent structure connecting evidence nodes (factor reuse) and, in the full DLN instantiation, a model-revision cycle over $\mathcal{M}$.	Collective decoding on $\bigotimes_{k\in A}\mathcal{E}_k$; Chernoff-optimal exponents are feasible when m-copy coherence is available.

4 Optimal decoding and Chernoff sample complexity

4.1 Binary hypothesis testing on fragments

Fix an SBS reference state $\sigma_{S\mathcal{E}}$ of the form (1) with $\mathcal{X} = \{0, 1\}$. For any fragment set $A \subseteq \{1, \ldots, N\}$, let

$$\sigma_A^{(x)} := \bigotimes_{k\in A} \sigma_{\mathcal{E}_k}^{(x)}$$

denote the conditional state of the accessible environment.

The observer first applies Λ_O to each accessed fragment and then performs an optimal measurement to decide x. This induces a binary quantum hypothesis testing problem:

$$H_0 :\ \rho_A = \bigotimes_{k\in A} \Lambda_O(\sigma_{\mathcal{E}_k}^{(0)}), \qquad H_1 :\ \rho_A = \bigotimes_{k\in A} \Lambda_O(\sigma_{\mathcal{E}_k}^{(1)}).$$

4.2 Quantum Chernoff bound and tight redundancy scaling

Define the (binary) quantum Chernoff coefficient for a pair of states ρ, σ:

$$Q(\rho, \sigma) := \min_{s\in[0,1]} \mathrm{Tr}\left[\rho^s \sigma^{1-s}\right],$$

and the associated Chernoff exponent

$$\xi(\rho, \sigma) := -\log Q(\rho, \sigma).$$

The quantum Chernoff bound states that for discriminating $\rho^{\otimes n}$ vs $\sigma^{\otimes n}$ with equal priors, the optimal error decays with exponent $\xi(\rho, \sigma)$ [15, 16].

We use a finite-n inequality that is convenient for sample-complexity statements.

Theorem 1 (Finite-n Chernoff upper bound)**.** *Let ρ, σ be density operators and consider equal priors on $H_0 : \rho$ and $H_1 : \sigma$. Then the optimal Bayes error obeys*

$$P_e^\star(\rho, \sigma) \le \tfrac{1}{2}\, Q(\rho, \sigma). \tag{3}$$

Consequently, for product states over a fragment set A,

$$P_e^\star\left(\bigotimes_{k\in A}\rho_k, \bigotimes_{k\in A}\sigma_k\right) \le \tfrac{1}{2}\min_{s\in[0,1]}\prod_{k\in A}\mathrm{Tr}\left[\rho_k^s\sigma_k^{1-s}\right].$$

Proof. Inequality (3) is a standard consequence of the Audenaert et al. bound and is commonly stated as $P_e^\star(\rho,\sigma) \le \frac{1}{2}\min_{s\in[0,1]}\mathrm{Tr}[\rho^s\sigma^{1-s}]$ [15]. The product form follows from multiplicativity of the trace under tensor products. □

Definition 6 (Observer-effective Chernoff exponent on a fragment set)**.** For an observer O and fragment set A, define

$$\xi_O(A) := \max_{s\in[0,1]}\left(-\sum_{k\in A}\log\mathrm{Tr}\left[\Lambda_O(\sigma_{\mathcal{E}_k}^{(0)})^s\,\Lambda_O(\sigma_{\mathcal{E}_k}^{(1)})^{1-s}\right]\right). \tag{4}$$

Proposition 1 (Access threshold as an information budget)**.** *Fix an error target $\delta\in(0,\frac{1}{2})$ and an SBS reference experiment. If an observer can access at most $m_{\max}=\lfloor R_O N\rfloor$ fragments, then a sufficient condition for δ-decoding of the pointer value is the existence of a set A with $|A|\le m_{\max}$ such that*

$$\xi_O(A) \ge \log\left(\frac{1}{2\delta}\right).$$

Proof. By Theorem 1, $P_e^\star(A) \le \frac{1}{2}\exp(-\xi_O(A))$. If $\xi_O(A)\ge\log(1/(2\delta))$, then $P_e^\star(A)\le\delta$. □

4.3 Calibration as distinguishability contraction

A central point for "non-ideal observers" is that calibration noise cannot improve distinguishability. For the Chernoff coefficient, this is a data-processing statement.

Theorem 2 (Calibration degrades Chernoff distinguishability)**.** *Let Λ be a CPTP map and ρ,σ quantum states. For every $s\in[0,1]$,*

$$\mathrm{Tr}\left[\Lambda(\rho)^s\Lambda(\sigma)^{1-s}\right] \;\ge\; \mathrm{Tr}\left[\rho^s\sigma^{1-s}\right].$$

Equivalently, $Q(\Lambda(\rho),\Lambda(\sigma)) \ge Q(\rho,\sigma)$ and therefore

$$\xi(\Lambda(\rho),\Lambda(\sigma)) \le \xi(\rho,\sigma).$$

Proof. For $s\in(0,1)$, define the Petz-Rényi divergence $D_s(\rho\|\sigma)=\frac{1}{s-1}\log\mathrm{Tr}[\rho^s\sigma^{1-s}]$. For $s\in(0,1)$ this divergence satisfies the data-processing inequality $D_s(\Lambda(\rho)\|\Lambda(\sigma))\le D_s(\rho\|\sigma)$ under CPTP maps [19, 22, 23]; see also Polyanskiy and Wu [24] for strong data-processing refinements. Rearranging yields the claimed inequality for $\mathrm{Tr}[\cdot]$. The endpoint cases $s=0,1$ follow by continuity. □

5 ε-SBS robustness of decision rules

The point of an explicit trace-distance SBS approximation is that it immediately controls *any* decision procedure via data processing.

Lemma 1 (Decision-theoretic continuity under trace distance)**.** *Let ρ and σ be two states on the same Hilbert space and let* Dec *be any (possibly adaptive) measurement-plus-decision procedure outputting a discrete hypothesis $\widehat{X}$. Then*

$$\left|\mathbb{P}_\rho(\widehat{X}\ne X) - \mathbb{P}_\sigma(\widehat{X}\ne X)\right| \le D_{\mathrm{tr}}(\rho,\sigma).$$

Proof. A measurement-plus-decision procedure is a CPTP map from states to a classical distribution on $\widehat{X}$. Trace distance contracts under CPTP maps, so the total variation distance between the induced classical distributions is bounded by $D_{\mathrm{tr}}(\rho, \sigma)$ [14]. The error event $\{\widehat{X} \neq X\}$ is a measurable subset of outcomes, hence its probability differs by at most the total variation distance. □

Theorem 3 (ε-robust Chernoff sample complexity)**.** *Let $\rho_{S\mathcal{E}}$ be ε-SBS with witness $\sigma_{S\mathcal{E}}$. Fix a fragment set A and an observer O. Let $\delta \in (0, \frac{1}{2})$ be a target error under the* actual *state ρ.*

If $\xi_O(A) \geq \log\left(\frac{1}{2(\delta-\varepsilon)}\right)$ and $\delta > \varepsilon$, then there exists a decision procedure on A (namely the optimal decoder for the witness experiment) such that

$$\mathbb{P}_\rho(\widehat{X} \neq X) \leq \delta.$$

Proof. Apply Proposition 1 to the witness state σ: with the given $\xi_O(A)$, there exists a decoder achieving $\mathbb{P}_\sigma(\widehat{X} \neq X) \leq \delta - \varepsilon$. Then Lemma 1 gives $\mathbb{P}_\rho(\widehat{X} \neq X) \leq (\delta - \varepsilon) + \varepsilon = \delta$. □

6 Local versus collective decoding: a sharp gap for pure records

Observer temporal limitations often restrict *which measurements are feasible*. A key example is the distinction between collective measurements across m fragments (requiring quantum memory for coherence) and product measurements (measuring each fragment immediately).

For two pure states $|\psi_0\rangle, |\psi_1\rangle$ with overlap $c := |\langle\psi_0|\psi_1\rangle| \in (0, 1)$, the m-copy conditional states are $|\psi_0\rangle^{\otimes m}$ and $|\psi_1\rangle^{\otimes m}$ with overlap c^m. The quantum Chernoff coefficient is c^{2m}, giving exponent $-\log c^2$ per copy.

By contrast, any measurement on a *single copy* induces classical distributions p, q whose Bhattacharyya coefficient $B(p, q) = \sum_y \sqrt{p(y)q(y)}$ is bounded below by the square-root fidelity [25, 26]. For pure states this yields $B(p, q) \geq c$. For product measurements on m copies, the classical Chernoff coefficient is at least c^m, yielding exponent at most $-\log c$ per copy.

Corollary 1 (A factor-of-two exponent gap for pure-state records)**.** *Let $|\psi_0\rangle, |\psi_1\rangle$ be pure states with overlap $c \in (0, 1)$. Let $P_e^{\mathrm{coll}}(m)$ be the optimal Bayes error using* collective *measurements on m copies, and let $P_e^{\mathrm{prod}}(m)$ be the optimal Bayes error over all* product *measurements (local POVMs on each copy, followed by optimal classical postprocessing). Then the optimal error exponents satisfy*

$$\lim_{m\to\infty} -\frac{1}{m}\log P_e^{\mathrm{coll}}(m) = -\log(c^2), \qquad \limsup_{m\to\infty} -\frac{1}{m}\log P_e^{\mathrm{prod}}(m) \leq -\log(c).$$

In particular, the best achievable exponent under product measurements is at most half the collective-measurement exponent.

Proof. The collective-measurement exponent is the quantum Chernoff exponent for pure states, which equals $-\log(c^2)$ [15, 16]. For product measurements, first measure each copy with some POVM, inducing classical distributions with Bhattacharyya coefficient $B \geq c$ [25, 26]. For i.i.d. classical samples, the classical Chernoff coefficient equals $\min_{s\in[0,1]} \sum_y p(y)^s q(y)^{1-s} \geq B$ (since $s = 1/2$ is feasible and gives B). Thus the m-sample coefficient is at least c^m, giving exponent at most $-\log c$. □

Remark 2 (Interpretation for observer quality)**.** The product-measurement bound $-\log c$ is *tight*: it is achieved by the Helstrom measurement applied independently to each copy, since the single-copy Bhattacharyya coefficient equals c for pure states [25]. Thus the factor-of-two gap is exact, not merely an artifact of the upper-bound technique. If τ_O is too small to maintain coherence

across many fragments, the observer is effectively restricted to product measurements, reducing the achievable redundancy by this quantifiable amount. This provides a mathematically explicit route from temporal observer constraints to reduced objectivity.

7 Worked physical model: central-spin pure dephasing

We now provide a concrete open-system model and compute (R_O, C_O, τ_O) in terms of physical parameters.

7.1 Model

Let S be a qubit with pointer basis the eigenbasis of σ_z^S. Let the environment consist of N qubits with $\sigma_z^{(k)}$. Consider the pure-dephasing Hamiltonian

$$H = \sigma_z^S \otimes \sum_{k=1}^{N} g_k \sigma_z^{(k)}, \tag{5}$$

and initial environment state $|+\rangle^{\otimes N}$ with $|+\rangle = (|0\rangle + |1\rangle)/\sqrt{2}$. Conditioned on the pointer value $x \in \{0, 1\}$ (eigenvalues ± 1 of σ_z^S), fragment k evolves to a pure state

$$|\phi_k^{(x)}(t)\rangle = e^{\mp i g_k t \sigma_z} |+\rangle ,$$

so that the single-fragment overlap is

$$c_k(t) := \left| \langle \phi_k^{(0)}(t) \rangle \, \phi_k^{(1)}(t) \right| = |\cos(2 g_k t)| . \tag{6}$$

This model (and its variants) is standard in decoherence theory and is directly connected to SBS formation in spin environments [5, 27, 28].

7.2 Exact Chernoff exponent and fragment requirement

For pure states, the Chernoff coefficient equals the fidelity:

$$Q\left(|\phi_k^{(0)}(t)\rangle , |\phi_k^{(1)}(t)\rangle \right) = c_k(t)^2, \qquad \xi_k(t) = -\log c_k(t)^2.$$

For a set A of accessed qubits,

$$\xi(A; t) = \sum_{k \in A} -\log\left(\cos^2(2 g_k t) \right) , \tag{7}$$

and Theorem 1 implies

$$P_e^\star(A; t) \leq \tfrac{1}{2} \exp(-\xi(A; t)) .$$

Thus a sufficient condition for error $\leq \delta$ is $\xi(A; t) \geq \log(1/(2\delta))$.

7.3 Mapping to observer parameters

Access fraction R_O. In a laboratory implementation, an observer may only intercept a fraction of environment qubits (geometric coverage, detector efficiency, spatial range). If $m_{\max}$ qubits are accessible per trial out of N, then $R_O = m_{\max}/N$.

Calibration C_O. Suppose the observer's instrument applies a depolarizing channel on each accessed environment qubit: $\Lambda_p(\rho) = (1-p)\rho + p\frac{\mathbf{1}}{2}$, capturing miscalibration or noise before readout. For any two qubit states, depolarization contracts trace distance by a factor $(1-p)$ [14]. For the central-spin conditional pure states, the single-copy Helstrom success probability becomes

$$C_O(t) = \tfrac{1}{2}\left(1 + (1-p)\sqrt{1 - c_k(t)^2}\right) = \tfrac{1}{2}\left(1 + (1-p)|\sin(2g_k t)|\right),$$

where we used $c_k(t) = |\cos(2g_k t)|$. If couplings differ, $C_O(t)$ varies with k and can be summarized by a worst-case or average calibration across accessible fragments.

Temporal horizon τ_O. If the observer performs collective decoding across m fragments, a quantum memory must preserve coherence for at least the acquisition time of those m qubits plus the decoding time. Let t_{meas} be the per-qubit acquisition time. A minimal feasibility constraint is $\tau_O \gtrsim m\, t_{\text{meas}}$. Additionally, the pointer value must remain stable over the acquisition interval, typically limited by system relaxation times (e.g., T_1) [29, 30]. In this model, we treat stability as an explicit constraint rather than assuming exponential pointer stability a priori.

7.4 Numerical illustration and reproducibility

The accompanying repository includes a script that samples couplings $\{g_k\}$, computes $\xi(A;t)$ for the best accessible subset under an access fraction R_O, and plots redundancy as a function of time t. This script is provided to ensure full reproducibility of the worked example. Figure 1 shows a typical redundancy profile as a function of interaction time in this toy model.

8 DLN-series connection and stage mapping

This paper can be read independently as a finite-resource analysis of observer-limited decoding in the QD/SBS setting. Nevertheless, it is motivated by a broader program in which "observer quality" is treated as a property of the *information-processing topology* used to integrate evidence. In the Dot–Linear–Network (DLN) compression model, stage differences are formalized by two objects: (i) a *belief-dependency graph* G (a directed acyclic graph in the sense of Pearl [31]) governing how evidence updates propagate at the inference level, and (ii) a *revision graph* $\mathcal{R}$ over a model space $\mathcal{M}$ governing when an observer can revise its representational assumptions [10].

The three q-states introduced in Sec. 3.3 provide an operational instantiation of these stages for quantum Darwinism: q_{D} corresponds to memoryless single-fragment decoding (no persistent dependency structure), q_{L} corresponds to product decoding with classical aggregation (independent evidence nodes), and q_{N} corresponds to collective decoding that exploits the shared latent pointer record as an explicit common factor (Table 1). In this physics setting, the resource triple $Q_O = (R_O, \Lambda_O, \tau_O)$ determines which q-state is feasible by constraining access, calibration, and the time available to maintain coherence across fragments.

We emphasize that DLN is used here as a representational classification and a source of modeling priors for bounded observers. The quantitative claims of this paper (Chernoff-based sample complexity, calibration contraction, and ε-robustness) are self-contained and do not presuppose any developmental interpretation. Rather than deferring structural revision, we incorporate the DLN revision graph directly: we define an observer-specific revision topology $\mathcal{R}_O$ over admissible decoder models and show that its topological features (notably the presence or absence of a directed cycle) control dynamical redundancy and pointer accessibility in non-stationary QD/SBS protocols (Sec. 9).

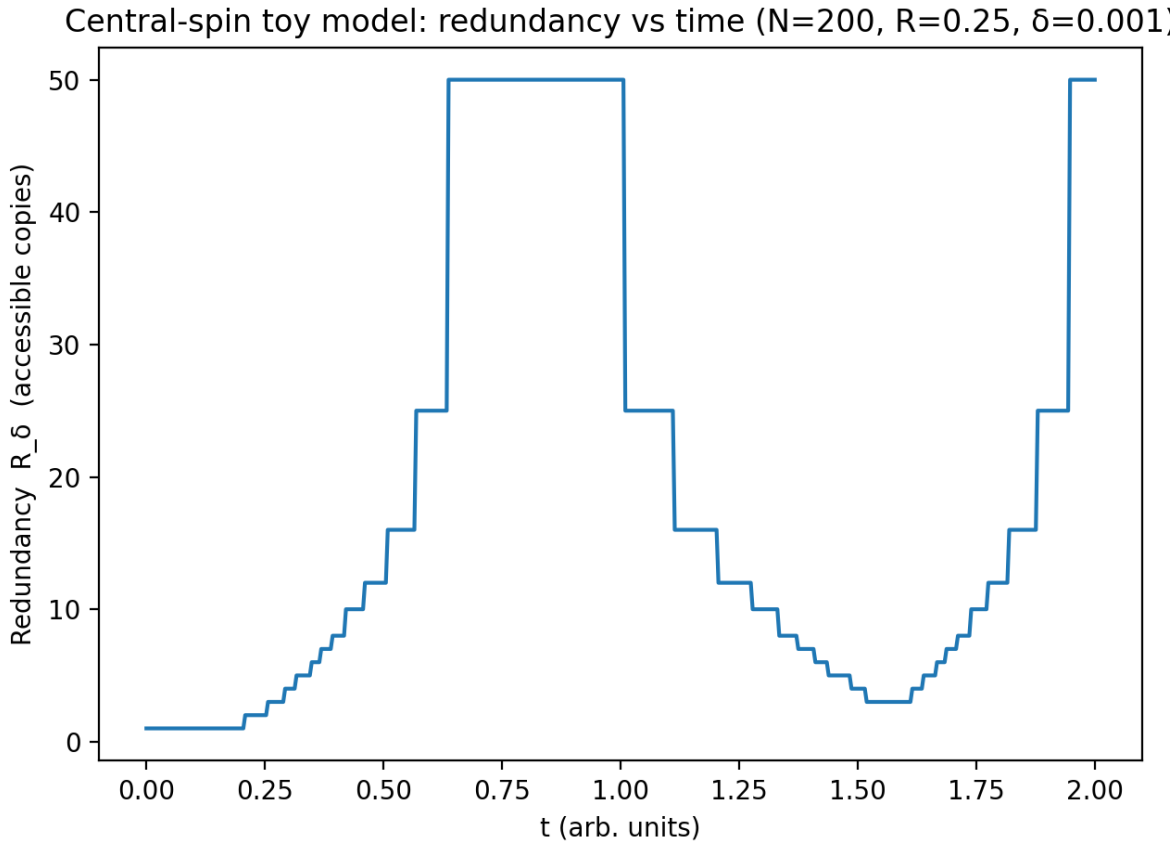

Figure 1: Central-spin toy model (Sec. 7): redundancy (accessible copies) versus interaction time t for a sampled distribution of couplings $\{g_k\}$, access fraction $R_O = 0.25$, and target decoding error $\delta = 10^{-3}$. The curve is produced by the reproducibility script in the repository.

9 Observer topology and three new results

The preceding sections treat observer quality as a *within-episode* resource constraint: for a fixed SBS witness experiment, the observer chooses a decoder class (Sec. 3.3) and incurs sample complexity governed by a Chernoff-type exponent that contracts under calibration noise and remains stable under ε-SBS perturbations. Here we add the DLN second layer: a *revision topology* that constrains how an observer can revise its decoding assumptions across time in a non-stationary observation model (cf. the temporal monitoring perspective of Mironowicz et al. [32]). This yields three results that are not visible in a purely static analysis.

9.1 Non-stationary regimes, revision topology, and monitoring

We model an experiment as a sequence of episodes $t = 1, 2, \ldots$. In episode t the observer attempts to infer a pointer variable $X_t \in \mathcal{X}$ from an m-fragment register A_t. The conditional fragment states may vary over time due to drift, coherence loss, or regime switching. We capture this by an unobserved regime parameter $\theta_t \in \Theta$, with conditional joint states $\rho_{A_t}^{(x)}(\theta_t)$. The observer may deploy a decoder from a class $q \in \{q_{\mathrm{D}}, q_{\mathrm{L}}, q_{\mathrm{N}}\}$, but in general the *appropriate* decoder depends on θ_t.

Definition 7 (Observer revision graph)**.** Let $\mathcal{M}$ be a set of decoder models (or decoding assumptions) available to an observer, e.g., $\mathcal{M} = \{\mathrm{Dec}_{\mathrm{L}}, \mathrm{Dec}_{\mathrm{N}}\}$ for product versus collective decoding. The *observer revision graph* is a directed graph

$$\mathcal{R}_O = (\mathcal{M}, \mathcal{T}_O), \qquad \mathcal{T}_O \subseteq \mathcal{M} \times \mathcal{M},$$

whose edges specify which model switches the observer can execute between episodes. We call $\mathcal{R}_O$ *expand-only* if $\mathcal{R}_O$ is acyclic (no directed cycle), and *full-cycle* if $\mathcal{R}_O$ contains a directed cycle.

In the DLN framework, $\mathrm{Dec}_{\mathrm{N}}$ corresponds to a factorized representation in which fragments share a latent pointer record, while $\mathrm{Dec}_{\mathrm{L}}$ corresponds to an expanded representation in which fragments are treated independently. An expansion transition $\mathrm{Dec}_{\mathrm{N}} \to \mathrm{Dec}_{\mathrm{L}}$ is triggered by detected failure of the shared-latent assumption; a contraction transition $\mathrm{Dec}_{\mathrm{L}} \to \mathrm{Dec}_{\mathrm{N}}$ is triggered when diagnostic evidence supports restoring coherent joint processing.

Definition 8 (Monitoring action and monitoring cost)**.** A *monitoring action* is any procedure that produces an estimate $\widehat{\theta}_t$ of the current regime parameter θ_t with misclassification probability at most η_t. We model monitoring as consuming an episode budget fraction $C_{\mathrm{monitor}} \in (0, 1)$, leaving an effective decoding budget fraction $1 - C_{\mathrm{monitor}}$ for inferring X_t. Operationally, C_{monitor} can represent: (i) a fraction of fragments reserved for diagnostic tests, (ii) an acquisition-time overhead that reduces usable coherence window, or (iii) calibration work that reduces integration time.

Principle 1 (Monitoring is never free)**.** *In non-stationary observation models, any policy that keeps the probability of applying a regime-inappropriate decoder exponentially small in the fragment budget necessarily incurs a nonzero monitoring cost* $C_{\mathrm{monitor}} > 0$.

Remark 3 (Why Principle 1 is operationally unavoidable)**.** To adapt between regimes with exponentially small failure probability, the observer must distinguish regimes with exponentially small misclassification probability. If each diagnostic fragment yields a positive Chernoff information $\xi_{\mathrm{diag}} > 0$ for testing $\theta \in \{\theta^{\mathrm{good}}, \theta^{\mathrm{bad}}\}$, then achieving $\eta_t \le e^{-\beta m}$ requires at least $m_{\mathrm{diag}} \ge (\beta/\xi_{\mathrm{diag}})m$ diagnostic fragments. Thus $C_{\mathrm{monitor}} = m_{\mathrm{diag}}/m \ge \beta/\xi_{\mathrm{diag}} > 0$. The value of C_{monitor} is a physical parameter determined by the diagnostic channel and the reliability requirement.

9.2 Result A: dynamical redundancy depends on revision topology

We quantify long-run performance using a time-averaged effective error exponent. Let $P_{e,t}$ be the episode-t decoding error for inferring X_t. Define the effective exponent

$$\xi_{\mathrm{eff}} := \liminf_{T\to\infty} \left(-\frac{1}{Tm} \sum_{t=1}^{T} \log(2P_{e,t}) \right). \tag{8}$$

Remark 4 (Ensemble versus typical effective exponent)**.** For i.i.d. regime draws, ξ_{eff} converges almost surely to the *typical* (quenched) exponent $\mathbb{E}[-(1/m)\log(2P_{e,t})]$ by the strong law of large numbers. A distinct quantity is the *ensemble* (annealed) exponent

$$\xi_{\mathrm{ens}} := -\frac{1}{m} \log\big(2\,\mathbb{E}[P_{e,t}]\big),$$

which characterizes the decay rate of the *average* error probability across episodes. By Jensen's inequality applied to the concave function $x \mapsto \log x$,

$$\xi_{\mathrm{ens}} \;\le\; \xi_{\mathrm{eff}},$$

with equality when $P_{e,t}$ is deterministic (e.g. for regime-robust product decoding). The gap can be substantial: under the unmonitored binary model, $\xi_{\text{eff}} = f\,\xi_{\text{N}}/m > 0$ for all $f > 0$ (Theorem 4(iii) with $\xi_{\text{garbage}} = 0$), while $\xi_{\text{ens}} \to 0$ as $m \to \infty$ because the average error saturates at $(1-f)/2$. Theorems 4–5 are stated in terms of ξ_{eff}; the numerical verification (Sec. 9.6) reports both quantities where they differ.

For a fixed regime θ, define the best achievable *per-fragment* exponents within decoder classes by

$$\xi_{\text{L}}(\theta) := \limsup_{m\to\infty} -\frac{1}{m}\log\big(2P^{\star}_{e,\text{L}}(m;\theta)\big), \qquad \xi_{\text{N}}(\theta) := \lim_{m\to\infty} -\frac{1}{m}\log\big(2P^{\star}_{e,\text{N}}(m;\theta)\big),$$

where $P^{\star}_{e,\text{L}}$ is the optimal error under product measurements (class q_{L}) and $P^{\star}_{e,\text{N}}$ is the optimal error under collective measurements (class q_{N}) when feasible.

Theorem 4 (Dynamical redundancy as a topological invariant of $\mathcal{R}_O$)**.** *Assume a two-regime model $\theta_t \in \{\theta^{\text{good}}, \theta^{\text{bad}}\}$ with $\mathbb{P}(\theta_t = \theta^{\text{good}}) = f \in (0,1)$ i.i.d. over episodes. Assume that in the good regime collective decoding strictly improves the exponent, $\xi_{\text{N}}(\theta^{\text{good}}) > \xi_{\text{L}}(\theta^{\text{good}})$, while in the bad regime product decoding is robust and dominates any fixed, unmonitored collective decoder in the sense that there exists a "stale" collective decoder $\text{Dec}^{\text{stale}}_{\text{N}}$ with exponent $\xi_{\text{garbage}} := \liminf_{m\to\infty} -\frac{1}{m}\log(2P^{\text{stale}}_{e}(m;\theta^{\text{bad}})) < \xi_{\text{L}}(\theta^{\text{bad}})$. Then:*

(i) ***Full-cycle.*** *If $\mathcal{R}_O$ contains a directed cycle enabling $\text{Dec}_{\text{L}} \leftrightarrows \text{Dec}_{\text{N}}$ and the observer monitors regimes with cost $C_{\text{monitor}} > 0$ and exponentially small misclassification probability, then there exists a policy achieving*

$$\xi_{\text{eff}} \;\geq\; (1 - C_{\text{monitor}})\Big(f\,\xi_{\text{N}}(\theta^{\text{good}}) + (1-f)\,\xi_{\text{L}}(\theta^{\text{bad}})\Big).$$

(ii) ***Expand-only.*** *If $\mathcal{R}_O$ is expand-only with an absorbing linear state (no contraction edge $\text{Dec}_{\text{L}} \to \text{Dec}_{\text{N}}$), and if $\mathbb{P}(\theta_t = \theta^{\text{bad}}) > 0$, then any policy that avoids using $\text{Dec}^{\text{stale}}_{\text{N}}$ on bad-regime episodes must eventually remain in Dec_{L}, and hence*

$$\xi_{\text{eff}} = \xi_{\text{L}}(\theta^{\text{bad}}) \quad \textit{(permanently, after a transient).}$$

(iii) ***Fixed collective decoding without monitoring.*** *If the observer applies $\text{Dec}^{\text{stale}}_{\text{N}}$ in every episode without monitoring, then*

$$\xi_{\text{eff}} = f\,\xi_{\text{N}}(\theta^{\text{good}}) + (1-f)\,\xi_{\text{garbage}},$$

which can be arbitrarily small and may be negative if $P^{\text{stale}}_{e}(m;\theta^{\text{bad}}) > 1/2$ for large m.

Proof sketch. (i) Under full-cycle $\mathcal{R}_O$ with monitoring cost C_{monitor}, the observer reserves a fraction C_{monitor} of each episode's fragment budget for regime diagnostics and applies Dec_{N} or Dec_{L} on the remaining $(1-C_{\text{monitor}})m$ fragments according to the monitoring outcome. By the i.i.d. assumption and the strong law of large numbers applied to the per-episode log-errors, the time-averaged exponent converges a.s. to f times the good-regime contribution plus $(1-f)$ times the bad-regime contribution, each evaluated on $(1-C_{\text{monitor}})m$ fragments. (ii) If $\mathcal{R}_O$ is acyclic with absorbing state Dec_{L}, then the first bad-regime episode triggers the irreversible transition $\text{Dec}_{\text{N}} \to \text{Dec}_{\text{L}}$. Since $\mathbb{P}(\theta_t = \theta^{\text{bad}}) > 0$, this transition occurs in finite time a.s., after which every episode uses Dec_{L}. (iii) Without monitoring, the observer applies $\text{Dec}^{\text{stale}}_{\text{N}}$ in every episode. In good-regime episodes (fraction f) the exponent is $\xi_{\text{N}}(\theta^{\text{good}})$; in bad-regime episodes (fraction $1-f$) it is ξ_{garbage}. The SLLN gives the claimed weighted average. □

Remark 5 (Interpretation)**.** Result A establishes that long-run redundancy is not determined solely by within-episode access, calibration, and memory, but also by whether the observer can *complete a revision cycle* after a period of operating under a robust (expanded) decoding assumption. The key invariant is topological: the existence of a directed cycle in $\mathcal{R}_O$ separates observers that can recover high-exponent collective decoding from observers that irreversibly collapse to the linear baseline.

9.3 Result B: inverted sophistication below a critical coherence fraction

Result B identifies a regime in which a collective measurement—despite being strictly more powerful under ideal conditions—yields higher error than product decoding when deployed without coherence monitoring. The mechanism is a mismatch between the measurement design (which presupposes inter-fragment coherence) and the actual regime (which may lack it).

Theorem 5 (Inverted sophistication threshold for unmonitored collective decoding)**.** *In the setting of Theorem 4, define*

$$f^\star := \frac{\xi_{\mathrm{L}}(\theta^{\mathrm{bad}}) - \xi_{\mathrm{garbage}}}{\xi_{\mathrm{N}}(\theta^{\mathrm{good}}) - \xi_{\mathrm{garbage}}} \;\in\; (0,1),$$

assuming $\xi_{\mathrm{garbage}} < \xi_{\mathrm{L}}(\theta^{\mathrm{bad}}) < \xi_{\mathrm{N}}(\theta^{\mathrm{good}})$*. If the coherence fraction satisfies* $f < f^\star$*, then the unmonitored stale collective decoder is strictly worse than optimal product decoding in the sense that*

$$\xi_{\mathrm{eff}}(\mathrm{Dec}_{\mathrm{N}}^{\mathrm{stale}}) < \xi_{\mathrm{eff}}(\mathrm{Dec}_{\mathrm{L}}^{\star}) = \xi_{\mathrm{L}}(\theta^{\mathrm{bad}}),$$

even though collective decoding is optimal in the good regime.

Proof. Under unmonitored stale collective decoding, $\xi_{\mathrm{eff}} = f\,\xi_{\mathrm{N}}(\theta^{\mathrm{good}}) + (1-f)\,\xi_{\mathrm{garbage}}$ (Theorem 4(iii)). Optimal product decoding achieves exponent $\xi_{\mathrm{L}}(\theta^{\mathrm{bad}})$ in both regimes by robustness (assumption). Rearranging the inequality $f\,\xi_{\mathrm{N}}(\theta^{\mathrm{good}}) + (1-f)\,\xi_{\mathrm{garbage}} < \xi_{\mathrm{L}}(\theta^{\mathrm{bad}})$ yields $f < f^\star$. □

Remark 6 (Per-episode versus time-averaged thresholds)**.** Theorem 5 characterizes the *time-averaged* effective exponent ξ_{eff}, yielding a threshold $f^\star$ that depends on the per-fragment exponents but not on the fragment count m. A complementary *per-episode* analysis considers the single-episode error probability $P_e^{\mathrm{un}}(m) = f\,P_e^N(m) + (1-f)/2$ and defines $f^*_{\mathrm{episode}}(m) := (P_e^L(m) - 1/2)/(P_e^N(m) - 1/2)$. Since $P_e^N(m) \to 0$ exponentially faster than $P_e^L(m)$, the per-episode threshold satisfies $f^*_{\mathrm{episode}}(m) \to 1$ as $m \to \infty$, with $1 - f^*_{\mathrm{episode}} \sim \exp(-\xi_L\, m)$. Thus the per-episode formulation predicts that for any fixed $f < 1$, there exists m^* beyond which *every individual episode* of unmonitored collective decoding has higher error than product decoding.

Remark 7 (Physical meaning of f and ξ_{garbage})**.** In a laboratory realization, f can be realized either as a *time fraction* of coherent episodes (interspersed with decohered episodes) or as an effective coherence parameter induced by storing an m-fragment register for time τ_O before a collective measurement. A simple model is an observer-memory dephasing channel with $f = e^{-\gamma\tau_O}$. The "garbage" exponent ξ_{garbage} is defined operationally as the error exponent achieved by a collective POVM optimized for a coherent register when applied to a decohered one; it quantifies the performance degradation incurred by unmonitored sophistication.

9.4 Robustness of inverted sophistication: observer-side versus system-side decoherence

The inverted sophistication threshold $f^\star$ depends on the physical mechanism by which coherence is lost. We distinguish two classes and verify that the qualitative prediction is robust to the choice of decoherence model, while its quantitative strength is not.

Definition 9 (Observer-side versus system-side decoherence)**.** Let $\{|\phi_k^{(x)}\rangle\}$ denote the conditional fragment states in an SBS witness experiment.

(i) *Observer-side decoherence.* The fragment states remain pure, but the observer's measurement apparatus fails to maintain the inter-fragment coherence required by the collective POVM. With probability $1-f$, the collective measurement returns an uninformative outcome; the product measurement, which acts on each fragment independently, is unaffected.

(ii) *System-side decoherence.* The fragment states themselves degrade via a depolarizing channel: $\sigma_k^{(x)} = f\,|\phi_k^{(x)}\rangle\langle\phi_k^{(x)}| + (1-f)\,I/2$. Both collective and product measurements operate on the same mixed-state register and are degraded symmetrically.

We analyze three concrete instantiations of the decoherence mechanism:

(a) **Binary episode-level (observer-side).** With probability f the collective POVM succeeds (error P_e^N); with probability $1-f$ it returns a random outcome ($P_e = 1/2$). The per-episode error is $P_e^{\text{un}} = f\,P_e^N + (1-f)/2$. The per-episode critical coherence fraction satisfies $f^*_{\text{episode}}(m) \to 1$ exponentially as $m \to \infty$, with $1 - f^*_{\text{episode}} \sim \exp(-\xi_L\, m)$.

(b) **Continuous exponent scaling (observer-side).** Partial decoherence reduces the effective collective exponent to $f\,\xi_N$. The time-averaged critical coherence fraction is $f^\star = \xi_L/\xi_N$. For pure-state records where $\xi_N = 2\,\xi_L$, this gives $f^\star = 1/2$ independent of m.

(c) **Fragment depolarization (system-side).** Both measurement classes operate on the depolarized states $\sigma_k^{(x)}$. The quantum Chernoff exponent for the collective measurement on the depolarized register remains strictly larger than the Helstrom exponent for product measurements at every $f \in (0, 1]$. *No inversion occurs*: the collective decoder retains its factor-of-two advantage uniformly.

Remark 8 (Physical interpretation)**.** The absence of inversion under system-side decoherence and its presence under observer-side decoherence is consistent with the observer-quality thesis: the inverted sophistication effect is a property of the *observer's measurement apparatus*, not of the environment's state. Product measurements are inherently robust to apparatus decoherence because they require no inter-fragment quantum coherence. Collective measurements exploit such coherence when it is available but suffer catastrophically when it is absent and undetected. This asymmetry is precisely what the revision graph $\mathcal{R}_O$ is designed to manage: a full-cycle topology enables the observer to detect coherence loss and fall back to the robust product strategy. More generally, the no-inversion property—$P_e^{\text{coll}} \le P_e^{\text{prod}}$—holds for arbitrary system-side CPTP noise, since $\text{Dec}_{\text{L}} \subset \text{Dec}_{\text{N}}$ and both decoder classes operate on the same noisy register. (The collective-versus-product exponent *gap* may, however, shrink or vanish under channels that render the conditional states effectively classical; the depolarization model of item (c) preserves a strictly positive gap because it does not alter the eigenbasis structure of the conditional states.)

9.5 Result C: pointer accessibility and observer-relative einselection

Result C formalizes a stage-dependent *resolution limit*: for finite fragment budgets, the DLN stage determines which pointer distinctions are operationally recoverable from environment fragments.

Definition 10 (Stage-conditional pointer accessibility)**.** Fix a fragment budget m and target error $\delta \in (0, 1/2)$. Let Π be a candidate pointer partition (a coarse-graining of $\mathcal{X}$) and let $\{\rho_A^{(\pi)}\}$ be the induced conditional fragment states for $\pi \in \Pi$. We say that Π is (m, δ)-*accessible* to an observer in

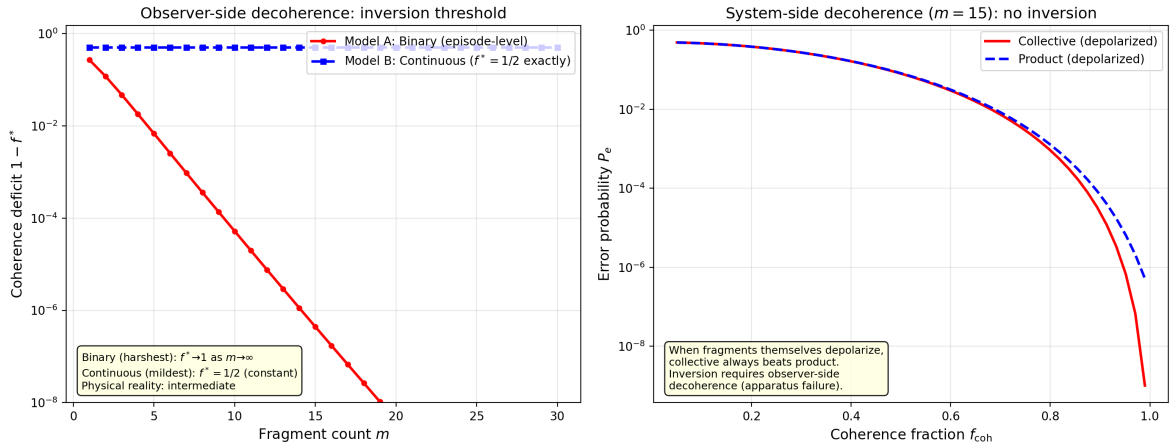

Figure 2: Robustness of inverted sophistication across decoherence models. *Left:* Critical coherence fraction $1 - f^*$ versus fragment count m for two observer-side models—binary (episode-level, $f^* \to 1$) and continuous (exponent-scaling, $f^* = 1/2$). Both predict inversion below f^*. *Right:* Under system-side depolarization, the collective decoder (solid) maintains strictly lower error than the product decoder (dashed) at all $f \in (0, 1]$, confirming the absence of inversion when decoherence is not observer-specific.

decoder class q if there exists a decoder in class q acting on m fragments whose worst-case error over $\pi \in \Pi$ is at most δ. Let $\mathfrak{P}(q; m, \delta)$ denote the set of all (m, δ)-accessible pointer partitions under class q.

Proposition 2 (Pointer accessibility gap across DLN stages)**.** *There exist SBS witness experiments and target accuracies* (m, δ) *for which*

$$\mathfrak{P}(q_{\mathrm{L}}; m, \delta) \subsetneq \mathfrak{P}(q_{\mathrm{N}}; m, \delta).$$

In particular, for pure-state records with overlap $c \in (0, 1)$*, any pointer distinction that requires an exponent exceeding* $-\log c$ *is inaccessible under product decoding within budget* m *but can be accessible under collective decoding because the achievable exponent can reach* $-\log(c^2)$ *(Cor. 1).*

Proof sketch. The inclusion $\subseteq$ holds because any product decoder is a special case of a collective decoder on the same register. Strictness follows by choosing a record model where the error target δ and budget m satisfy $m(-\log(c^2)) \geq \log(1/(2\delta))$ but $m(-\log c) < \log(1/(2\delta))$. Then collective decoding can meet the target while product decoding cannot, by Cor. 1. □

Corollary 2 (Observer-relative einselection under fragment constraints)**.** *If multiple approximately stable pointer partitions are supported by the same environment but differ in required fragment budget, then the* operationally objective *pointer partition selected by an observer depends on* (q_O, τ_O) *through the accessibility sets* $\mathfrak{P}(q_O; m, \delta)$*. In this sense, "einselection" can be formulated as a constrained optimization over pointer partitions, and designing the observer (its DLN stage and revision topology) selects which pointer distinctions are controllably accessible from a given fragment budget.*

9.6 Numerical verification in the central-spin model

We verify Results A–C in the central-spin pure-dephasing model of Sec. 7 with $N = 200$ environment qubits, couplings $g_k \sim \mathrm{Uniform}(0.8, 1.2)$, interaction time $t = 0.5$, and monitoring fraction $C_{\mathrm{monitor}} =$

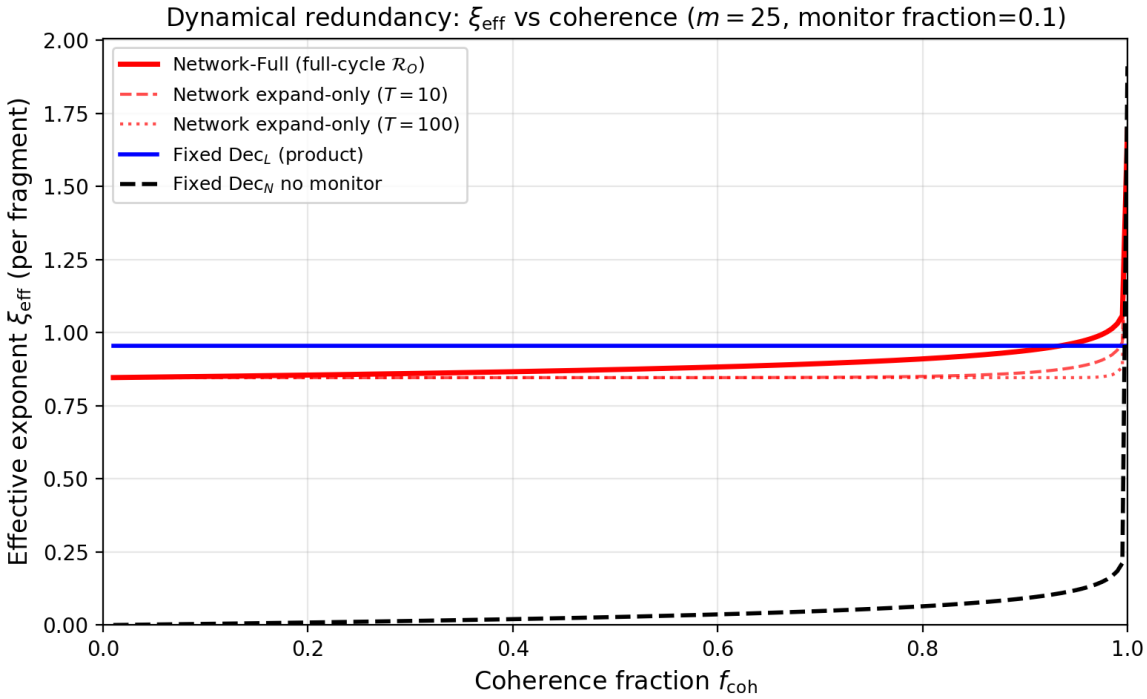

Figure 3: Result A: per-episode ensemble exponent ξ_{ens} (Remark 4) as a function of coherence fraction f for four observer types in the central-spin model ($m = 25$, $C_{\text{monitor}} = 0.10$). Network-Full (full-cycle $\mathcal{R}_O$) maintains a positive exponent for all $f \in (0, 1)$, while the unmonitored-collective ensemble exponent collapses toward zero as the average error is dominated by failed episodes. The monitoring cost produces a visible gap between Full-cycle and the product baseline.

0.10. The accompanying repository contains scripts that reproduce all numerical results and figures reported below.

Result A (dynamical redundancy). At $m = 25$ fragments, the per-fragment collective and product exponents are $\xi_N/m = 1.91$ and $\xi_L/m = 0.96$, confirming the ratio $\xi_N/\xi_L = 2.00$. At coherence fraction $f = 0.8$, the per-episode ensemble exponents (Remark 4) are: $\xi^{\text{Full}}_{\text{ens}} = 0.91$ (full-cycle), $\xi^{L}_{\text{ens}} = 0.96$ (fixed product), and $\xi^{\text{un}}_{\text{ens}} = 0.06$ (unmonitored collective). The corresponding typical exponents from Theorem 4 are $\xi^{L}_{\text{eff}} = 0.96$ (unchanged, as product decoding is regime-robust) and $\xi^{\text{un}}_{\text{eff}} = f\,\xi_{\text{N}}/m = 1.53$. The large gap $\xi^{\text{un}}_{\text{ens}} \ll \xi^{\text{un}}_{\text{eff}}$ reflects the dominance of failed episodes: although 80% of episodes achieve the collective exponent, the *average* error probability is controlled by the $(1-f)$-fraction in which coherence fails and the outcome is uninformative ($P_e = 1/2$). The full-cycle exponent is strictly positive under both measures for all $f \in (0, 1)$, and the monitoring cost (10% of fragments) produces a quantifiable gap below the product baseline—confirming Principle 1 and Theorem 4. See Fig. 3.

Result B (inverted sophistication). The per-episode critical coherence fraction under the binary model satisfies $f^*_{\text{episode}}(5) = 0.993$, $f^*_{\text{episode}}(10) = 0.9999$, and $f^*_{\text{episode}}(m) \to 1$ for $m \geq 15$. Under the continuous model, $f^\star = 0.50$ independent of m. Under system-side depolarization, the collective decoder maintains strictly lower error than the product decoder at all $f \in (0, 1]$ and all

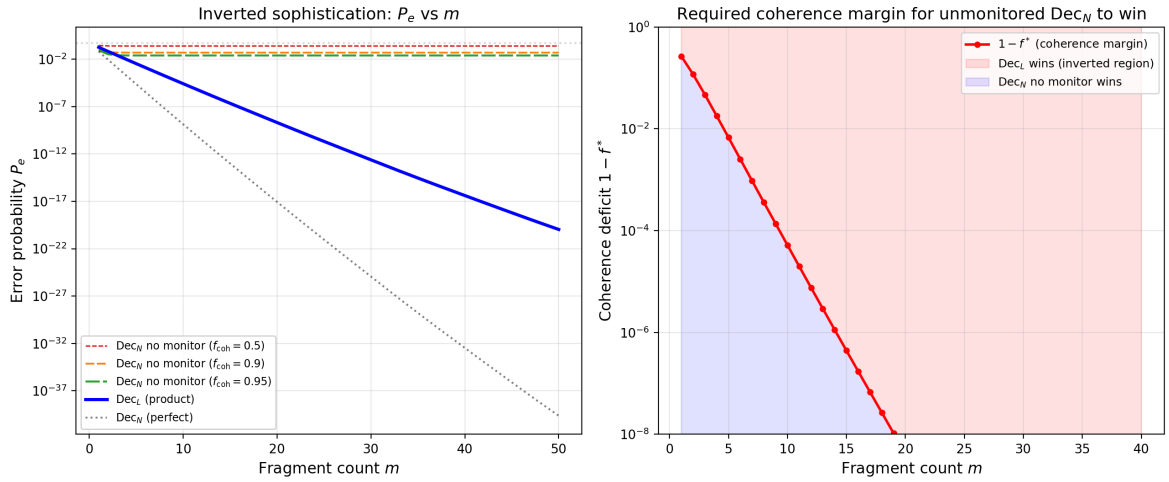

Figure 4: Result B: inverted sophistication crossover. *Left:* Error probability versus fragment count m for product (Dec_L) and unmonitored collective (Dec_N) decoders at representative coherence fractions. Below the critical f^*, the collective decoder has *higher* error than the product decoder. *Right:* Convergence of $1 - f^*_{\mathrm{episode}}(m)$ on a logarithmic scale, showing the exponential approach $f^* \to 1$ predicted by Theorem 5.

tested fragment counts $m \in \{5, 10, 15, 20, 25\}$, confirming the absence of inversion (Sec. 9.4). See Fig. 4.

Result C (pointer accessibility). With $m = 8$ fragments and error target $\delta = 10^{-3}$, the resolution gap (time points where q_N resolves the pointer but q_L does not) covers 19.6% of the time domain. The gap fraction decreases monotonically with m: 17.6% at $m = 12$, 10.0% at $m = 25$, and 3.0% at $m = 50$, consistent with Proposition 2(c). See Fig. 5.

10 Discussion: tightness, limitations, and relation to prior work

The main redundancy bound employs Chernoff-optimal decoding [15, 16] and explicitly incorporates calibration via a CPTP contraction theorem (Thm. 2) and ε-SBS perturbations (Thm. 3). The local-versus-collective decoding gap (Cor. 1) provides a quantitative link between temporal observer constraints and reduced error exponents.

The inverted sophistication threshold (Result B) is robust to the choice of decoherence model in the following precise sense: under any observer-side decoherence mechanism, there exists a critical coherence fraction below which unmonitored collective decoding is strictly inferior to product decoding. The quantitative threshold ranges from $f^\star = 1/2$ (continuous model) to $f^\star \to 1$ (binary model). Under system-side decoherence (fragment depolarization), no inversion occurs, confirming that the effect is a property of the observer's measurement apparatus rather than of the environment's state (Sec. 9.4).

The present work complements several strands in the QD literature: hazy environments [7], photon redundancy [11, 12], generic objectivity [8, 9], and accessible-information approaches [17]. Where those works parameterize the environment or the system–environment coupling, we parameterize the observer and its decoding architecture. Section 7 provides a fully worked open-system example, and Sec. 9.6 verifies all three dynamical predictions numerically in the same model.

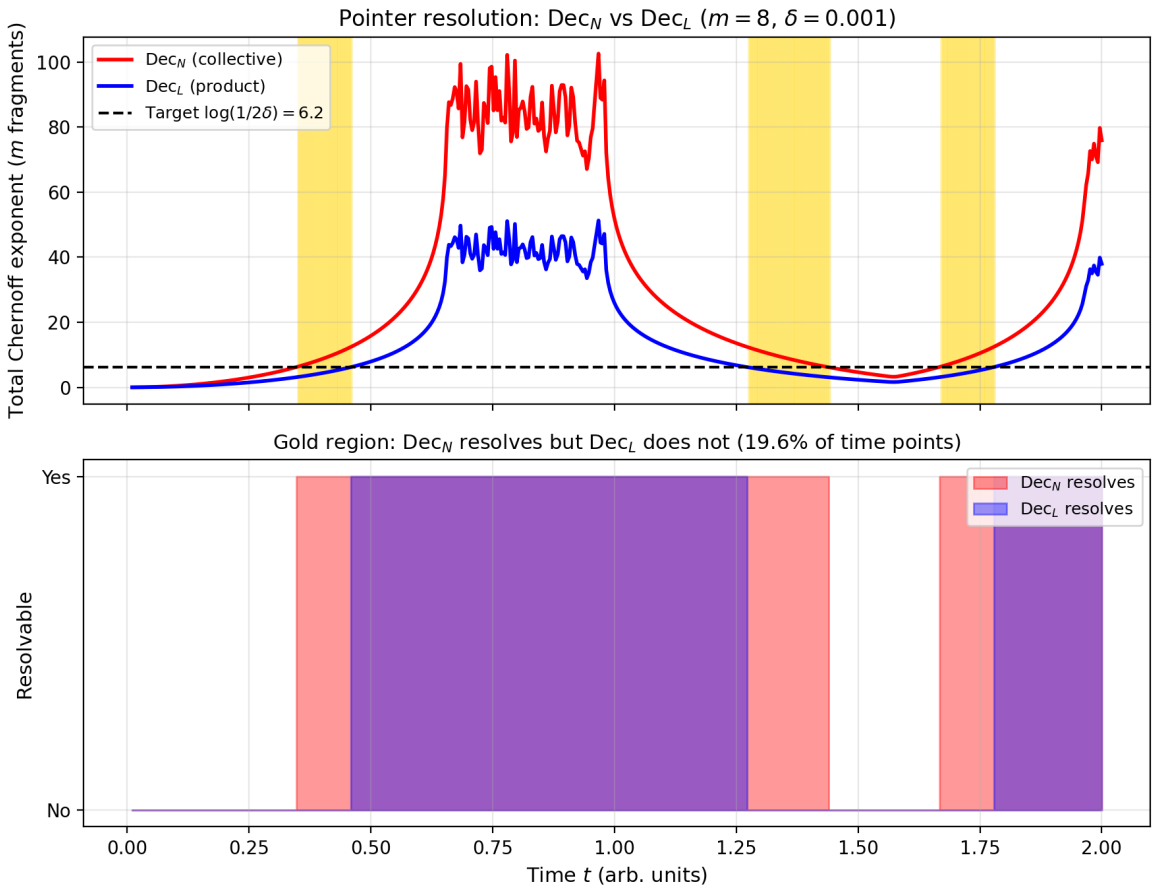

Figure 5: Result C: pointer resolution gap in the central-spin model. The shaded region indicates time windows where collective decoding (q_N) resolves the pointer distinction at error target $\delta = 10^{-3}$ but product decoding (q_L) does not. The gap fraction decreases with fragment budget m, vanishing as $m \to N$.

11 Conclusion

Observer modeling remains a structural gap in much of the QD/SBS literature. By treating the observer as a resource-constrained agent with explicit access, calibration, and temporal horizons, we obtain quantitative, decoder-level statements about redundancy and objectivity that remain stable under ε-SBS trace-distance approximations. The central-spin worked example demonstrates how these parameters can be computed from physical couplings and instrument noise, enabling model-to-experiment predictions.

The three dynamical predictions of Sec. 9 extend the static analysis to non-stationary observation protocols. The revision-graph topology $\mathcal{R}_O$ determines whether an observer can maintain a positive long-run Chernoff exponent under fluctuating coherence (Result A), predicts a regime in which unmonitored collective decoding is strictly inferior to product decoding (Result B), and identifies stage-dependent resolution limits on pointer accessibility (Result C). The robustness analysis of Sec. 9.4 establishes that the inverted sophistication effect is specific to observer-side decoherence, providing a testable distinction between apparatus limitations and environment-state degradation.

These results suggest that the observer's information-processing topology—not merely its access,

calibration, or temporal horizon—is a first-class resource in quantum Darwinism. Characterizing and controlling this topology may enable the design of measurement protocols that achieve near-optimal redundancy under realistic, non-stationary conditions.

References

[1] Harold Ollivier, David Poulin, and Wojciech H. Zurek. Objective properties from subjective quantum states: Environment as a witness. *Physical Review Letters*, 93:220401, 2004. doi: 10.1103/PhysRevLett.93.220401.

[2] Wojciech H. Zurek. Quantum darwinism. *Nature Physics*, 5:181–188, 2009. doi: 10.1038/nphys1202.

[3] Robin Blume-Kohout and Wojciech H. Zurek. Quantum darwinism: Entanglement, branches, and the emergent classicality of redundantly stored quantum information. *Physical Review A*, 73:062310, 2006. doi: 10.1103/PhysRevA.73.062310.

[4] R. Horodecki, J. K. Korbicz, and P. Horodecki. Quantum origins of objectivity. *Physical Review A*, 91:032122, 2015. doi: 10.1103/PhysRevA.91.032122.

[5] J. K. Korbicz. Roads to objectivity: Quantum darwinism, spectrum broadcast structures, and strong quantum darwinism – a review. *Quantum*, 5:571, 2021. doi: 10.22331/q-2021-11-08-571.

[6] Thao P. Le and Alexandra Olaya-Castro. Strong quantum darwinism and strong independence are equivalent to spectrum broadcast structure. *Physical Review Letters*, 122:010403, 2019. doi: 10.1103/PhysRevLett.122.010403.

[7] Michael Zwolak, H. T. Quan, and Wojciech H. Zurek. Quantum darwinism in a hazy environment. *Physical Review Letters*, 103:110402, 2009. doi: 10.1103/PhysRevLett.103.110402.

[8] Fernando G. S. L. Brandão, Marco Piani, and Paweł Horodecki. Generic emergence of classical features in quantum darwinism. *Nature Communications*, 6:7908, 2015. doi: 10.1038/ncomms8908.

[9] Paul A. Knott, Tommaso Tufarelli, Marco Piani, and Gerardo Adesso. Generic emergence of objectivity of observables in infinite dimensions. *Physical Review Letters*, 121:160401, 2018. doi: 10.1103/PhysRevLett.121.160401.

[10] A. Wu. Compression efficiency and structural learning as a computational model of dln cognitive stages, 2026. Preprint (bioRxiv); DOI: 10.64898/2026.02.01.703168.

[11] C. Jess Riedel and Wojciech H. Zurek. Quantum darwinism in an everyday environment: Huge redundancy in scattered photons. *Physical Review Letters*, 105:020404, 2010. doi: 10.1103/PhysRevLett.105.020404.

[12] C. Jess Riedel and Wojciech H. Zurek. Redundant information from thermal illumination: Quantum darwinism in scattered photons. *New Journal of Physics*, 13:073038, 2011. doi: 10.1088/1367-2630/13/7/073038.

[13] C. W. Helstrom. *Quantum Detection and Estimation Theory*. Academic Press, 1976.

[14] John Watrous. *The Theory of Quantum Information*. Cambridge University Press, 2018. ISBN 9781316848142.

[15] K. M. R. Audenaert, M. Nussbaum, A. Szkoła, and F. Verstraete. Discriminating states: The quantum chernoff bound. *Physical Review Letters*, 98:160501, 2007. doi: 10.1103/PhysRevLett.98.160501.

[16] Michael Nussbaum and Arleta Szkoła. The chernoff lower bound for symmetric quantum hypothesis testing. *The Annals of Statistics*, 37(2):1040–1057, 2009. doi: 10.1214/08-AOS593.

[17] Akram Touil, Bin Yan, Davide Girolami, Sebastian Deffner, and Wojciech Hubert Zurek. Eavesdropping on the decohering environment: Quantum darwinism, amplification, and the origin of objective classical reality. *Physical Review Letters*, 128:010401, 2022. doi: 10.1103/PhysRevLett.128.010401.

[18] Mario A. Ciampini, Giorgia Pinna, Paolo Mataloni, and Mauro Paternostro. Experimental signature of quantum darwinism in photonic cluster states. *Physical Review A*, 98:020101, 2018. doi: 10.1103/PhysRevA.98.020101.

[19] Marco Tomamichel. *Quantum Information Processing with Finite Resources: Mathematical Foundations*, volume 5 of *SpringerBriefs in Mathematical Physics*. Springer, 2016. ISBN 978-3-319-21890-8. doi: 10.1007/978-3-319-21891-5.

[20] Koenraad M. R. Audenaert, Milán Mosonyi, and Frank Verstraete. Quantum state discrimination bounds for finite sample size. *Journal of Mathematical Physics*, 53(12):122205, 2012. doi: 10.1063/1.4768252.

[21] Hao-Chung Cheng, Nilanjana Datta, Nana Liu, Theshani Nuradha, Robert Salzmann, and Mark M. Wilde. An invitation to the sample complexity of quantum hypothesis testing. *npj Quantum Information*, 11:94, 2025. doi: 10.1038/s41534-025-00980-8.

[22] Dénes Petz. Quasi-entropies for finite quantum systems. *Reports on Mathematical Physics*, 23 (1):57–65, 1986. doi: 10.1016/0034-4877(86)90067-4.

[23] Milán Mosonyi and Tomohiro Ogawa. Quantum hypothesis testing and the operational interpretation of the quantum rényi relative entropies. *Communications in Mathematical Physics*, 334:1617–1648, 2015. doi: 10.1007/s00220-014-2248-x.

[24] Yury Polyanskiy and Yihong Wu. Strong data-processing inequalities for channels and bayesian networks, 2016. arXiv:1508.06025v4.

[25] Christopher A. Fuchs and Carlton M. Caves. Ensemble-dependent bounds for accessible information in quantum mechanics. *Physical Review Letters*, 73:3047–3050, 1994. doi: 10.1103/PhysRevLett.73.3047.

[26] Richard Jozsa. Fidelity for mixed quantum states. *Journal of Modern Optics*, 41(12):2315–2323, 1994. doi: 10.1080/09500349414552171.

[27] Kamil Roszak and Jarosław K. Korbicz. Entanglement and objectivity in pure dephasing models. *Physical Review A*, 100:062127, 2019. doi: 10.1103/PhysRevA.100.062127.

[28] Michael Zwolak, C. Jess Riedel, and Wojciech H. Zurek. Amplification, decoherence and the acquisition of information by spin environments. *Scientific Reports*, 6:25277, 2016. doi: 10.1038/srep25277.

[29] H.-P. Breuer and F. Petruccione. *The Theory of Open Quantum Systems*. Oxford University Press, 2002.

[30] Maximilian Schlosshauer. *Decoherence and the Quantum-to-Classical Transition*. Springer, 2007.

[31] Judea Pearl. *Probabilistic Reasoning in Intelligent Systems: Networks of Plausible Inference*. Morgan Kaufmann, 1988.

[32] Piotr A. Mironowicz, Jarosław K. Korbicz, and Paweł Horodecki. Monitoring of the process of system information broadcasting in time. *Physical Review Letters*, 118:150501, 2017. doi: 10.1103/PhysRevLett.118.150501.